Journal of Magnetism and Magnetic Materials 472 (2019) 53–58

Contents lists available at ScienceDirect

Journal of Magnetism and Magnetic Materials

journal homepage: www.elsevier.com/locate/jmmm

Research articles

Magnetic detection of nanoparticle sedimentation in magnetized ferrofluids

Alex van Silfhout, Ben Erné*

Van't Hoff Laboratory for Physical and Colloid Chemistry, Debye Institute for Nanomaterials Science, Utrecht University, The Netherlands

ARTICLE INFO

Keywords:
Ferrofluids
Magnetic nanoparticles
Colloidal stability
Sedimentation
X-ray transmission

ABSTRACT

Colloidal stability in external magnetic field is crucial for applications of ferrofluids. Here, we introduce a magnetic analysis approach to monitor how rapidly magnetic nanoparticles are pulled out of the liquid in an external magnetic field gradient. The motion of the sedimentation front is deduced from the time-dependent field produced by a column of ferrofluid placed on a permanent magnet. Citrate-stabilized nanoparticles in a homemade aqueous ferrofluid are found to sediment at the rate expected of single nanoparticles. More rapid sedimentation occurs in two other types of ferrofluid, indicating that our magnetic sedimentation analysis method can differentiate ferrofluids with respect to their in-field colloidal stability. Our method is further validated by comparison with time-dependent X-ray transmission profiles.

1. Introduction

Ferrofluids are concentrated colloidal dispersions of magnetic nanoparticles that behave as liquid magnets in external field. Oil-based ferrofluids are used as lubricants in many applications, with the advantage that they can be magnetically kept into place [1–5]. Another type of application of ferrofluids exploits the phenomenon of magnetic levitation: a nonmagnetic object that would sink in a normal liquid can be made to levitate in a ferrofluid, whose apparent mass density can be tuned via the magnetization of the fluid and via the magnetic field gradient [5]. Magnetic levitation has been applied for decades in the diamond industry, to separate diamonds from gangue material [6], and currently, magnetic levitation is being developed as a technology to separate solid waste materials for recycling [7]. The separation of plastics by magnetic density separation requires new low-cost high-stability ferrofluids that are water based, to prevent the dissolution of plastic.

For optimal colloidal stability of a ferrofluid, the magnetic nanoparticles must be dispersed at the single particle level and the pair interaction upon contact between two nanoparticles must be repulsive. The stability will thus depend on the magnitude of the nanoparticle dipole moments and on the modification of the surface with possibly charged chemical groups or surfactants [8–10]. Reversible or irreversible nanoparticle structures may already be present in zero field [11,12], they may grow in external field [13], and isotropic attraction between nanoparticles may result in macroscopic phase separation [14]. To guide the chemical development of new ferrofluids with optimal stability, it is important to have a method to characterize how rapidly the magnetic material settles towards a magnet. Moreover, this characterization should be done at the same magnetic field gradients and relatively high nanoparticle concentrations that are relevant for magnetic fluid applications. We note that precise knowledge of the magnetophoretic velocity of nanoparticles is also relevant in the framework of the magnetic capture of nanoparticles in microfluidic bioassay devices [15].

The measurement of magnetization curves is a favorite way to characterize ferrofluids, but it is not very informative about their colloidal aggregation state. With magnetic nanoparticles in the 5–10 nm diameter range prepared by coprecipitation, a magnetization curve will be largely the same whether the nanoparticles are single or clustered, as the particles mostly respond to the external field individually [16,17]. With larger nanoparticles that form dipolar structures in zero field and which grow in external field, the structures do affect the magnetization curve [18,19], but still the presence of nanoparticle structures cannot easily be deduced from the magnetization curve alone. Field-induced dipolar structures have been visualized by cryo-TEM [13], but this is neither a routine method and nor does it give a macroscopic characterization of stability. Small angle scattering of X-rays [20] or neutrons [21] can reveal dipolar structure formation in the presence or absence of a magnetic field, but it requires access to dedicated beam facilities. Optical imaging of a thin capillary in external field is a useful option that can be used not only to study sedimentation equilibrium profiles [22] but also to detect whether magnetophoresis is more rapid than expected in the absence of aggregates. Time-resolved optical detection of concentration profiles in external magnetic field can be applied to a wide range of systems, with particle sizes ranging from a few

* Corresponding author.
E-mail address: b.h.erne@uu.nl (B. Erné).

https://doi.org/10.1016/j.jmmm.2018.10.010
Received 20 June 2018; Received in revised form 12 September 2018; Accepted 1 October 2018
Available online 03 October 2018
0304-8853/

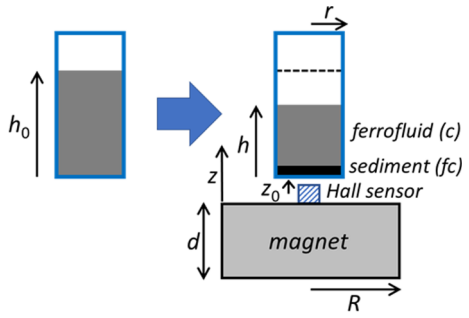

Fig. 1. Schematic of the proposed approach to monitor the sedimentation of magnetic nanoparticles in a ferrofluid towards a magnet. The ferrofluid of concentration c in a cylindrical flask of internal radius r is magnetized by the permanent magnet below and contributes to the magnetic field measured at a Hall effect sensor positioned between magnet and ferrofluid. In the simplest interpretation of the data, as the position h of the sedimentation front moves, a sediment of concentration fc is formed ($f > 1$), affecting the strength of the measured magnetic field.

nanometers up to several micrometers [23].

The approach that we propose here is to monitor the external magnetic field produced by a small bottle of ferrofluid placed on top of a permanent magnet. It is a convenient and simple approach that allows easy comparison of the in-field colloidal stability of different ferrofluids. In the Theory section, the principle of our method is described, together with our mathematical approach to calculate sedimentation rates from the time-dependent magnetic data. Practical aspects of our setup are presented in the Experimental section, and the Results and Discussion compare the colloidal stabilities of a few different ferrofluids in external field.

2. Theory

2.1. Magnetic analysis of sedimentation front position

Our approach to characterize the colloidal stability of ferrofluids in external field is summarized in Fig. 1. As a column of ferrofluid is placed on a permanent magnet, the liquid becomes a magnet itself. The dipoles of the magnetic nanoparticles become aligned to an extent that depends on the magnitudes of the dipole moments and on the strength of the external field. For simplicity, a cylindrical permanent magnet is used and we consider only its axial field H, given by [24]

$$H(z) = \frac{M}{2}\left[\left(\frac{z+d}{\sqrt{(z+d)^2+R^2}}\right)-\left(\frac{z}{\sqrt{z^2+R^2}}\right)\right] \quad (1)$$

Here M is the magnet's (internal) remanent magnetization, z is the distance from the top surface of the magnet, d is the magnet's thickness, and R is its radius.

The dimensions of the initial column of magnetized ferrofluid are given by the height h_0 of the liquid column and the internal radius r of the flask. As the nanoparticles sediment, the geometry changes. As a simple model, we propose to assume that the flask now contains three cylindrical layers: (1) a nonmagnetic top layer that starts at the position h of the sedimentation front, (2) a ferrofluid layer with the same concentration c as at the start of the experiment, and (3) a sediment layer of a constant, increased concentration. Because of the strong optical absorbance of the dilute ferrofluid that remains above the sedimentation front, its position is typically not visible to the naked eye. Nevertheless, the sedimentation can now be monitored from the field measured by a Hall sensor positioned in between the magnet and the column of ferrofluid. The measured field will combine the constant contribution of the permanent magnet and the time-dependent contribution of the sample.

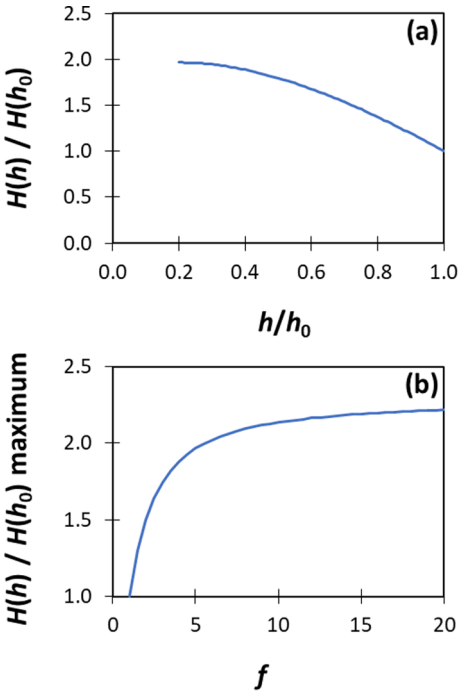

Fig. 2. (a) Calculation via Eq. (1) of the field H as a function of the position h of the sedimentation front scaled to the initial value ($h = h_0$) for a sediment whose concentration is increased by a factor $f = 5$ compared to the initial concentration. Dimensions of permanent magnet: 30 mm thickness, 22.5 mm radius. Dimensions of liquid column: 10 mm height, 6.5 mm radius, minimal distance to Hall sensor: 2 mm. (b) Maximum value of $H(h)/H(h_0)$ as a function of f, the relative concentration in the sediment compared to the initial ferrofluid.

In the framework of our simple model, the measured field originating from the sample consists of two contributions: the field from the sediment and the field from the ferrofluid below the sedimentation front. In this model, we assume a sediment of constant concentration, which increases in size over time. Here, we define a factor f, which gives the ratio between the concentration of the sediment and the concentration of the dispersion at the start of the experiment. In terms of Eq. (1), the sediment is a cylindrical magnet that starts at a distance z_0 from the Hall sensor and has a thickness d equal to $(h_0 - h)/(f - 1)$. The ferrofluid layer is a second cylindrical magnet, starting at a height $z_0 + (h_0 - h)/(f - 1)$ and with a thickness d equal to $h_0 - (h_0 - h)/(f - 1)$. In both cases, the radius R is the internal radius r of the flask. Finally, the magnetization M scales with c for the ferrofluid and with fc for the sediment. This assumes that the sediment and the ferrofluid are close to magnetic saturation.

Within the simple model, the measured field can be calculated from the position of the sedimentation front, and vice versa. The example calculation in Fig. 2a corresponds to our experimental geometry for a sediment that is more concentrated than the initial ferrofluid by a factor $f = 5$. Once sedimentation is complete, all particles are found in a pellet whose thickness is 1/5 of the initial height of the ferrofluid column, which is $(f-1) = 4$ times smaller than the resulting supernatant. A numerical expression for the measured field from the sample as a function of the position of the sedimentation front can be solved for h, giving an expression for the position of the sedimentation front in terms of the measured field. Different ferrofluids will have a different factor f by which the concentration of the sediment is enhanced compared to the initial dispersion, leading to a different final thickness of the sediment and a different final enhancement $H(h)/H(h_0)$ of the measured sample field compared to its initial value. Fig. 2b shows the final values of $H(h)/H(h_0)$ for f going from 1 to 20 in our measurement geometry; on this basis, the value of f in the case of a particular ferrofluid can be

determined from the final value of $H(h)/H(h_0)$.

2.2. Aggregation dependence of sedimentation rate

The sedimentation rate of single or aggregated magnetic nanoparticles in external magnetic field results from a balance between magnetic force and friction. Force of gravity is typically weaker by two orders of magnitude.

Upon full magnetic alignment of nanoparticle dipoles with external field, the magnetic force F_{mag} on a colloidal particle (single nanoparticle or aggregate) with a magnetic moment m_{colloid} is given by [25]

$$F_{mag} = \mu_0 m_{colloid} dH/dz \tag{2}$$

where μ_0 is the permeability of free space and dH/dz is the external magnetic field gradient. In practice, magnetic alignment will not be complete. When all magnetic nanoparticle dipoles are free to rotate thermally in zero field, the average degree of magnetic alignment in an external field H is described by the Langevin function: [26]

$$M/M_{\mathrm{sat}} = \coth(\alpha) - 1/\alpha \tag{3}$$

where M is the sample magnetization, M_{sat} is M at magnetic saturation, and $\alpha = \mu_0 mH/(kT)$, with μ_0 the permeability of free space, m the nanoparticle dipole moment, and kT the thermal energy. In our case, the gradient is found by taking the derivative of Eq. (1):

$$\frac{dH}{dz} = \frac{M}{2}\left[\left(\frac{\sqrt{(z+d)^2+R^2} - (z+d)^2[(z+d)^2+R^2]^{-1/2}}{(z+d)^2+R^2}\right) - \left(\frac{\sqrt{z^2+R^2} - z^2(z^2+R^2)^{-1/2}}{z^2+R^2}\right)\right] \tag{4}$$

The frictional force F_{friction} on a colloidal particle can be modelled in terms of the hydrodynamic radius a of an effective hard sphere: [27]

$$F_{friction} = 6\pi\eta a u \tag{5}$$

where η is the viscosity of the liquid medium on the colloidal particle scale and u is the velocity of the colloidal particle. Effects of non-spherical shape and hydrodynamic interactions are hidden in the value of the effective hydrodynamic radius. Moreover, this approach neglects back-diffusion, that is, diffusion in direction opposite to magnetophoresis due to the concentration gradient created by magnetophoresis; in our experiments, this assumption applies the best to the initial sedimentation rate, when the concentration profile is still far from reaching sedimentation-diffusion equilibrium.

With knowledge of colloidal size, dipole moment, viscosity, and field gradient, the magnetophoretic velocity u can be calculated. Conversely, the size of colloidal objects can be determined from the sedimentation rate. To obtain a rough estimate, we will assume the presence of colloidal particles of hydrodynamic radius a with an amount of magnetic material equal to a fraction x_{FeOx} of the total hydrodynamic volume. From $F_{\mathrm{mag}} = F_{\mathrm{friction}}$, Eqs. (2) and (5), and $m_{\mathrm{colloid}} = (4/3)\pi a^3 m_b x_{\mathrm{FeOx}}$ with m_{b} the bulk magnetization of iron oxide, the size of objects with a sedimentation rate u is given by

$$a \cong \sqrt{\frac{9\eta u}{2 m_b x_{\mathrm{FeOx}} \mu_0 (dH/dx)}} \tag{6}$$

Since the maximum possible fraction of magnetic material in a particle is 1, Eq. (6) gives a minimum effective size of the colloidal objects. Magnetic nanoparticles are expected to have a single magnetic domain, so that the magnetic moment of a particle with a diameter of 7 nm and a bulk magnetization of 430 kA/m [28] will be 7.7×10^{-20} Am^2. Bare single nanoparticle in water (viscosity: 10^{-3} Pas) in a gradient of 20 T/m are expected to sediment at a rate on the order of 0.08 mm per hour. From Eq. (6), much more rapid sedimentation will indicate the presence of aggregates containing many nanoparticles.

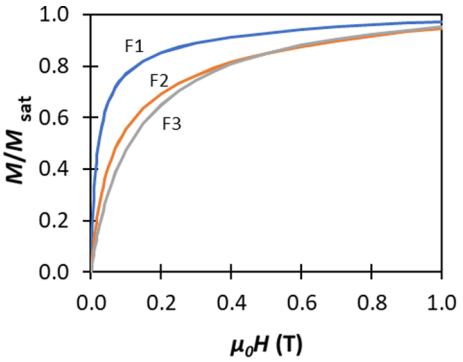

Fig. 3. Magnetization curve of ferrofluids F1, F2, and F3 measured by VSM. No hysteresis was observed, evidence of the superparamagnetic nature of the ferrofluid. Magnetization is scaled to the saturation magnetization of 12600, 2200, and 1140 A/m for F1, F2, and F3 respectively.

3. Experimental methods

Three different types of water-based ferrofluid were studied. Ferrofluids F1 and F2 were unfractionated prototype fluids of undisclosed precise origin (sterically stabilized iron oxide nanoparticles) kindly provided by the UMinCorp company (Rotterdam). Ferrofluid F3 contained citrate-stabilized maghemite nanoparticles at nearly neutral pH prepared by us via a recipe of Dubois et al. [14]. Magnetization curves were measured using a vibrating sample magnetometer (EZ-9 from Microsense, see example in Fig. 3) and particle sizes were determined using transmission electron microscopy (Tecnai 10, 100 kV). Both VSM and TEM indicated that F2 and F3 had particles with an average diameter of about 8 nm and about 30% polydispersity, typical for ferrofluids prepared by aqueous coprecipitation [29]. F1 had slightly larger particles, about 11 nm and about 30% polydispersity. The viscosity of the samples was measured at 20 °C in a cone-plate geometry (5 cm diameter, 1° cone angle) in the low-shear regime using a Physica Anton Paar MCR-300 rheometer.

A schematic of the setup used for magnetic analysis of ferrofluid sedimentation was shown in Fig. 1. A cylindrical neodymium magnet of 45 mm in diameter and 30 mm in thickness was obtained from SuperMagnete (Gottmadingen, Germany). A transverse Hall sensor probe with a square edge length of 1 mm (HMMT-6J04-VR, Lake Shore Cryotronics, Inc.) was fixed against the center of the magnet inside a thermostatized box consisting of a copper cylinder of 25 cm in diameter and 34 cm in depth kept close to the average temperature of the thermostatized room (typically 19.0 °C): water from a Julabo F25 cryostat was pumped through copper tubing welded onto the copper cylinder, itself contained in an insulated closed wooden box. Thermostatization within 0.1 °C is crucial for a stable background field from the neodymium magnet. Preliminary experiments indicated that the field from the neodymium magnet decreased by about 0.5 mT per temperature rise of 1 °C, and slight corrections were applied to subsequent measurements to take into account small changes in the measured temperature near the Hall probe. The sample consisted of a 4 mL glass vial with screw cap (VWR) 4.5 cm in height and 1.5 cm in external diameter (1.3 cm internal diameter) filled with 1.4 mL of ferrofluid and thermostatized overnight inside the box at 5 cm from the magnet center in lateral direction before it was slided onto the center of the magnet to start a measurement. The height of the liquid column from inside bottom of bottle to bottom of meniscus was 1.0 cm. Measurements with sample were performed for 100 h at 1 point per minute, after which the measurement was continued without sample for a few hours to verify the background field.

Fig. 4 shows the height-dependent axial field and gradient of our magnet (height dependence obtained by fixing the gauss probe onto a cathetometer with digital readout of the elevation). With the gauss

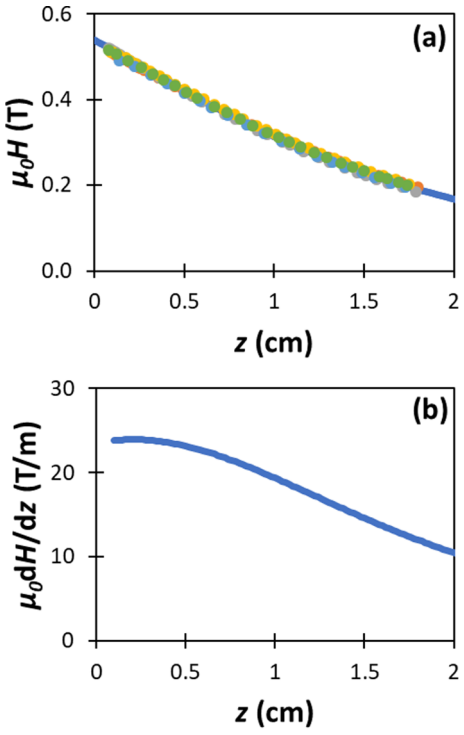

Fig. 4. (a) Measured axial field from our magnet as a function of the distance z from the surface. The fit is according to Eq. (1) ($\mu_0 M = 1.32$ T, $R = 0.0225$ m, $d = 0.030$ m). (b) Calculated axial magnetic field gradient of our magnet, see Eq. (4).

probe positioned against the magnet, the Hall sensor measured a field of 0.53 T, in line with the remanent magnetization of 1.32 T quoted by the supplier and a distance of ~1 mm between magnet surface and Hall sensor (inside the metal casing of the gauss probe). In the first cm above the magnet surface, the axial field drops to 0.32 T and the gradient is about 20 T/m.

To validate our calculation of magnetophoretic sedimentation rates from magnetic data, we also measured X-ray transmission profiles using a LUMiReader X-ray instrument (LUM, Berlin; 17.48 keV molybdenum X-ray source). A liquid column of 1 cm in height inside a plastic disposable cuvette (2 mm optical path length) was placed on the same type of magnet as used for the magnetic experiments. The X-ray absorbance from a water-filled cuvette was subtracted.

4. Results and discussion

Magnetic stability analyses of ferrofluid F1 are shown in Fig. 5, before and after dilution with water by factors of 2, 4, and 8. The initially measured field scales with the initial concentration (Fig. 5a), and the relative increase in field from the sample in 100 h is the largest at the highest dilution (Fig. 5b). In terms of the model presented in the Theory section, the most concentrated sample exhibits not only the slowest sedimentation but also seems to tend towards a less strongly sedimented sample upon prolonged sedimentation (Fig. 5c).

Similar measurements performed on ferrofluids F2 and F3 are shown in Fig. 6.

The observed differences in relative field increase as presented in Fig. 5b can be understood by comparing the data to X-ray measurements of the equilibrium concentration profiles in Fig. 7.

The profiles in Fig. 7 show that there is no full settling of the particles at the bottom of the sample. The density of the sediment increases towards the bottom, and the highest density is reached in the most concentrated sample. This can be understood in terms of a gradual increase in osmotic pressure towards the bottom of the sediment:

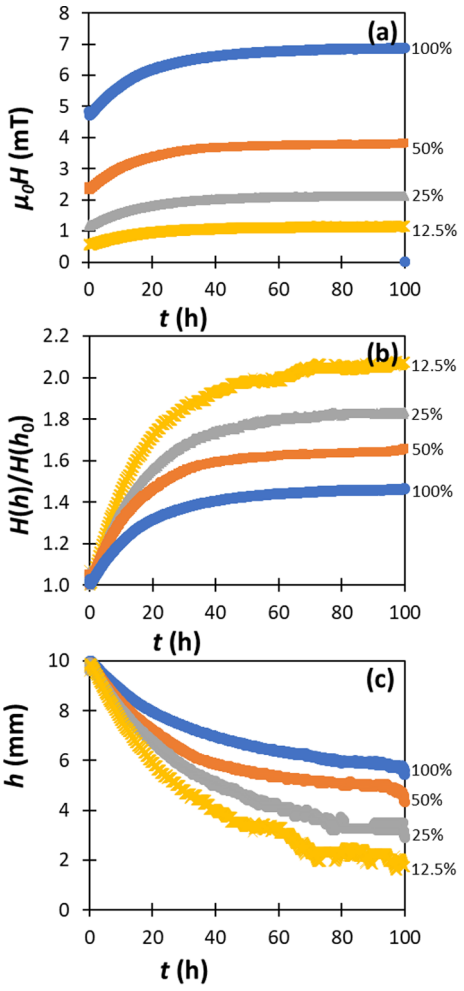

Fig. 5. (a) Measured fields from samples placed on a magnet, corrected for the background field of the magnet (~500.7 mT). Samples are F1 before dilution and after dilution by factors of 2, 4, and 8. (b) Measured fields relative to the initial sample field; final values of $H(h)/H(h_0)$ are 1.48, 1.65, 1.78, and 2.06, corresponding to f values of 1.8, 2.5, 3.3, and 6.8, respectively (see Fig. 2b). (c) Position of the sedimentation front as calculated by the model presented in Figs. 1 and 2. The initial sedimentation rates of the increasingly dilute samples are 0.13, 0.16, 0.20, and 0.23 mm per hour.

repulsive interactions that keep the particles apart gradually yield to the pressure exerted by the column of sediment above it [30,31].

The trend of increasing initial sedimentation rate upon dilution follows the trend of decreasing viscosity: values of 2.30, 1.46, 1.20, and 1.12 mPa.s were measured for dilution factors of 1, 2, 4, and 8, respectively. For comparison, ferrofluids F2 and F3 each had viscosities of 1.10 and 1.08 mPa.s, respectively. As the viscosities were measured without magnetic field and the volume fractions of magnetic material are low (2.6% for the most concentrated sample), the trend in viscosity is ascribed to the presence of excess polymer surfactant. At similar viscosity, ferrofluids F1 (0.23 mm/h) and F2 (0.19 mm/h) show more rapid sedimentation than F3 (0.06 mm/h), whose rate is close to that expected for single particles (0.08 mm/h, see Section 2.2). The more rapid sedimentation in F1 can in part be ascribed to the slightly larger nanoparticles in that system compared to F2 and F3. From Eq. (6), the colloidal objects in F2 have a radius that is larger than that of single particles by a factor of about 2, suggesting the presence of aggregates of a 5–10 nanoparticles.

Time-dependent X-ray transmission profiles of ferrofluid F1 are shown in Fig. 8a. For a comparison with the magnetic measurements, we used Eq. (1) to calculate the contribution from each elevation to the

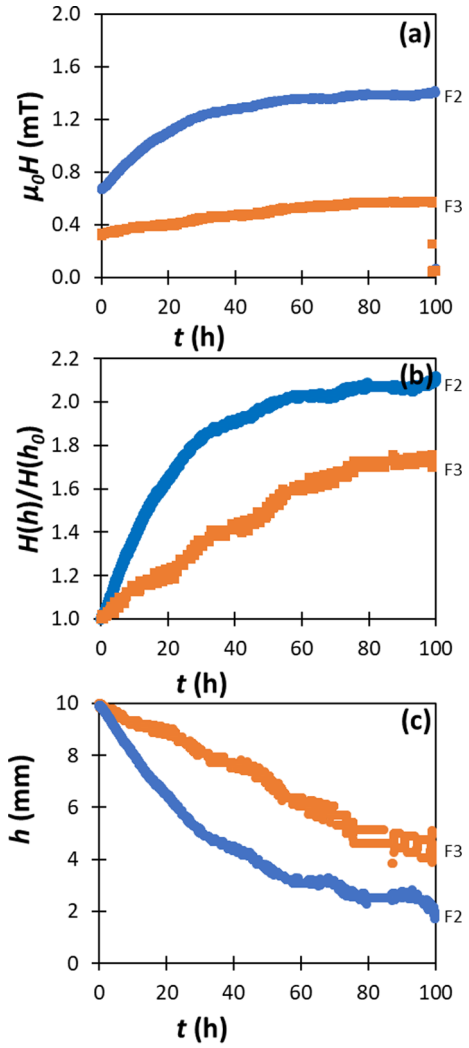

Fig. 6. As in Fig. 5, but for samples F2 and F3: (a) measured field corrected for background (~500.7 mT), (b) same data but now scaled to initial sample field, and (c) calculated position of the sedimentation front. In F2, $H(h)/H(h_0)$ reaches 2.05, corresponding to $f = 6.7$, and we find an initial sedimentation rate of 0.19 mm per hour. In F3, $H(h)/H(h_0)$ reaches 1.72 ($f = 3.1$), and we find a sedimentation rate of 0.06 mm per hour.

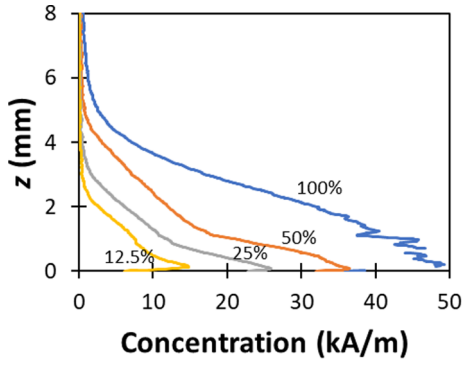

Fig. 7. Equilibrium concentration profiles of sample F1 before dilution and after dilution by factors of 2, 4, and 8. The undiluted fluid initially had a magnetization of 12600 A/m (initial ferrofluid height: 10 mm). Concentrations are given in terms of saturation magnetization, calculated from X-ray transmission and VSM measurements.

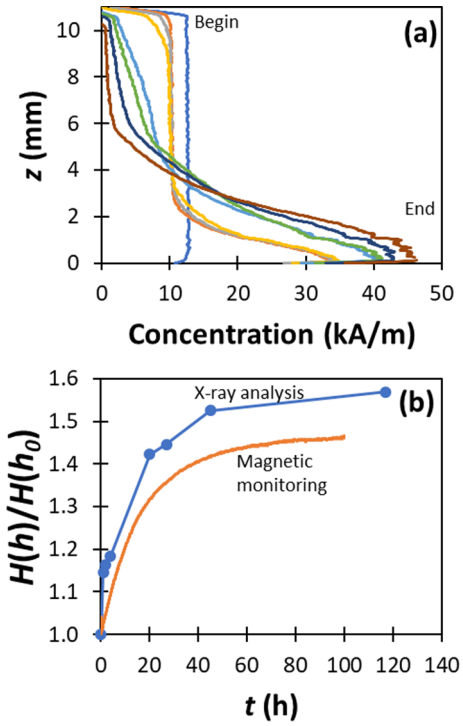

Fig. 8. (a) Time-dependent concentration profiles of undiluted sample F1. Each line is an average of two samples. (b) Relative increase in sample field due to sedimentation obtained from direct magnetic monitoring and calculated from the X-ray profiles in part (a) of this figure.

measured field, viewing the sample as a stack of disks each having a thickness given by the distance between two data points in the X-ray profile (about 13 μm) and a magnetization assumed to be linear with the X-ray absorbance and initially equal to the magnetization measured by VSM. The resulting predictions of the sample field at the position of the Hall sensor are shown in Fig. 8b.

The time-dependent increase in sample field calculated from X-ray profiles agrees with the magnetic measurement, except for a rapid initial increase in the first hour observed in the X-ray profiles but not in the magnetic measurements (Fig. 8b). This discrepancy does not result from incomplete magnetization of the sample, which causes the field to be about 10% lower than at saturation magnetization from start to finish of the experiment (see Fig. 3). About 20% of the magnetic material in this unfractionated ferrofluid can apparently easily be removed in external magnetic field before using the remaining fluid in applications. A possible reason why this fraction of the magnetic material is not observed in the magnetic measurements is that it consists of aggregates that already settle to the bottom during the temperature equilibration performed before starting the magnetic measurements. Lengthy equilibration is necessary for a stable background field from the permanent magnet, a drawback of the magnetic monitoring method. In future, a way might be found to perform the temperature equilibration with the sample much farther from the magnet.

5. Conclusions

Our magnetic approach to characterize the sedimentation rate of ferrofluids seems well suitable to compare the colloidal stability of ferrofluids in external magnetic field. Clear differences were observed between a ferrofluid with citrate-stabilized nanoparticles, which sedimented at the rate expected for single particles, and two other

ferrofluids in which sedimentation was more rapid. Moreover, a trend was observed in the sedimentation rate of a ferrofluid as a function of concentration, the slowest sedimentation occurring in the sample with the highest viscosity.

The descriptive model used in the magnetic analysis of sedimentation rates is oversimplified. X-ray transmission profiles indicate that the position of the sedimentation front is not abrupt but spread out and that the sediment does not have a homogeneous concentration but gradually becomes more concentrated towards the bottom. Nevertheless, further development of the magnetic sedimentation analysis method and its interpretation is not a priority. It is a simple method that measures a single parameter in time, the sample's contribution to the measured field, and it interprets the measurement in terms of a single parameter, the effective position of the sedimentation front. Development of a more elaborate model poses the risk of leading to overinterpretation. For more detailed information on the sedimentation process, a better approach seems to measure X-ray transmission profiles. In future work, we aim to focus on the interpretation of such profiles. In theory, they inform not only on the kinetics of sedimentation, but also on the colloidal interactions between the nanoparticles, since sedimentation equilibrium profiles can be used to calculate the osmotic equation of state [30,31].

Acknowledgements

The authors would like to thank Dominique Thies-Weesie for practical help and helpful discussions, Particle Solutions for help with the X-ray equipment, and Urban Mining Corporation for support and ferrofluid samples. This work is part of research programme P14-07, project number 3.1, (partly) financed by the Applied and Engineering Sciences branch of the Netherlands Organisation for Scientific Research (NWO-TTW).

References

[1] S. Odenbach, Colloidal Magnetic Fluids: Basics, Development and Application of Ferrofluids, Springer, Berlin, 2009.
[2] L. Vékás, D. Bica, M.V. Avdeev, Magnetic nanoparticles and concentrated magnetic nanofluids: synthesis, properties and some applications, China Part. 5 (2007) 43–49.
[3] C. Scherer, A.M. Figueiredo, Neto, ferrofluids: properties and applications, Braz. J. Phys. 35 (2005) 718–727.
[4] K. Raj, R. Moskowitz, Commercial applications of ferrofluids, J. Magn. Magn. Mater. 85 (1990) 233–245.
[5] R.E. Rosensweig, Ferrohydrodynamics, Cambridge University Press, 1985.
[6] L. Vatta, Floating diamonds with nanomagnetic particles, Macromol. Symp. 225 (2005) 221–228.
[7] S. Serranti, V. Luciani, G. Bonifazi, B. Hu, P. Rem, An innovative recycling process to obtain pure polyethylene and polypropylene from household waste, Waste Manage. 35 (2015) 12–20.
[8] B. Chanteau, J. Fresnais, J.-F. Berret, Electrosteric enhanced stability of functional sub-10 nm cerium and iron oxide particles in cell culture medium, Langmuir 25 (2009) 9064–9070.
[9] S. Laurent, D. Forge, M. Port, A. Roch, C. Robic, L. Vander Elst, R.N. Muller, Magnetic iron oxide nanoparticles: synthesis, stabilization, vectorization, physicochemical characterizations, and biological applications, Chem. Rev. 108 (2008) 2064–2110.
[10] C. Vasilescu, M. Latikka, K.D. Knudsen, V.M. Garamus, V. Socoliuc, R. Turcu, E. Tombácz, D. Susan-Resiga, R.H.A. Ras, L. Vékás, High concentration aqueous magnetic fluids: structure, colloidal stability, magnetic and flow properties, Soft Matter 14 (2018) 6648–6666.
[11] M. Klokkenburg, R.P.A. Dullens, W.K. Kegel, B.H. Erné, A.P. Philipse, Quantitative real-space analysis of self-assembled structures of magnetic dipolar colloids, Phys. Rev. Lett. 96 (2006) 037203.
[12] L.N. Donselaar, P.M. Frederik, P. Bomans, P.A. Buining, B.M. Humbel, A.P. Philipse, Visualisation of particle association in magnetic fluids in zero-field, J. Magn. Magn. Mater. 201 (1999) 58–61.
[13] M. Klokkenburg, B.H. Erné, J.D. Meeldijk, A. Wiedenmann, A.V. Petukhov, R.P.A. Dullens, A.P. Philipse, *In Situ* imaging of field-induced hexagonal columns in magnetite ferrofluids, Phys. Rev. Lett. 97 (2006) 185702.
[14] E. Dubois, V. Cabuil, F. Boué, R. Perzynski, Structural analogy between aqueous and oily magnetic fluids, J. Chem. Phys. 111 (1999) 7147–7160.
[15] M. Fratzl, S. Delshadi, T. Devillers, F. Bruckert, O. Cugat, N.M. Dempsey, G. Blaire, Magnetophoretic induced convective capture of highly diffusive superparamagnetic nanoparticles, Soft Matter 14 (2018) 2671–2681.
[16] R. Chantrell, J. Popplewell, S. Charles, Measurements of particle size distribution parameters in ferrofluids, IEEE Trans. Magn. 14 (1978) 975–977.
[17] A. Ivanov, S. Kantorovich, E. Reznikov, C. Holm, A. Pshenichnikov, A. Lebedev, A. Chremos, P.J. Camp, Magnetic properties of polydisperse ferrofluids: a critical comparison between experiment, theory, and computer simulation, Phys. Rev. E 75 (2007) 1–12.
[18] V. Mendelev, A. Ivanov, Magnetic properties of ferrofluids: an influence of chain aggregates, J. Magn. Magn. Mater. 289 (2005) 211–214.
[19] M. Klokkenburg, B.H. Erné, V. Mendelev, A.O. Ivanov, Magnetization behavior of ferrofluids with cryogenically imaged dipolar chains, J. Phys.-Condens. Matter 20 (2008) 204113.
[20] M. Bonini, E. Fratini, P. Baglioni, SAXS study of chain-like structures formed by magnetic nanoparticles, Mater. Sci. Eng. C 27 (2007) 1377–1381.
[21] M. Klokkenburg, B.H. Erné, A. Wiedenmann, A.V. Petukhov, A.P. Philipse, Dipolar structures in magnetite ferrofluids studied with small-angle neutron scattering with and without applied magnetic field, Phys. Rev. E 75 (2007) 051408.
[22] J.-F. Berret, O. Sandre, A. Mauger, Size distribution of superparamagnetic particles determined by magnetic sedimentation, Langmuir 23 (2007) 2993–2999.
[23] O. Mykhaylyk, D. Lerche, D. Vlaskou, V. Schoemig, T. Detloff, D. Krause, M. Wolff, T. Joas, S. Berensmeier, C. Plank, Magnetophoretic velocity determined by space- and time-resolved extinction profiles, IEEE Magn. Lett. 6 (2015) 1700104.
[24] H.D. Young, R.A. Freedman, University Physics, Pearson Education Inc., San Fancisco, 2004.
[25] Q.A. Pankhurst, J. Connolly, S.K. Jones, J. Dobson, Applications of magnetic nanoparticles in biomedicine, J. Phys. D: Appl. Phys. 36 (2003) R167–R181.
[26] P. Langevin, Sur la Théorie du Magnétisme, J. Phys. Theor. Appl. 4 (1905) 678–693.
[27] P.C. Hiemenz, R. Rajagopalan, Principles of Colloid and Surface Chemistry, M. Dekker, 1986.
[28] B.D. Cullity, Introduction to Magnetic Materials, Addison-Wesley, 1972.
[29] B. Luigjes, S.M.C. Woudenberg, R. de Groot, J.D. Meeldijk, H.M. Torres Galvis, K.P. de Jong, A.P. Philipse, B.H. Erné, Diverging geometric and magnetic size distributions of iron oxide nanocrystals, J. Phys. Chem. C 115 (2011) 14598–14605.
[30] B. Luigjes, D.M.E. Thies-Weesie, B.H. Erné, A.P. Philipse, Sedimentation equilibria of ferrofluids: II. Experimental osmotic equations of state of magnetite colloids, J. Phys.-Condens. Matter 24 (2012) 245104.
[31] B. Luigjes, D.M. Thies-Weesie, A.P. Philipse, B.H. Erné, Sedimentation equilibria of ferrofluids: I. Analytical centrifugation in ultrathin glass capillaries, J. Phys.-Condes. Matter 24 (2012) 245103.